GA–A22141

ELECTRON CYCLOTRON HEATING AND CURRENT DRIVE IN ITER

by

R.W. HARVEY, W.M. NEVINS, G.R SMITH,
B. LLOYD, M.F. O'BRIEN, and C.D. WARRICK

MARCH 1996

GA–A22141

ELECTRON CYCLOTRON HEATING AND CURRENT DRIVE IN ITER

by

R.W. HARVEY, W.M. NEVINS,* G.R SMITH,*
B. LLOYD,** M.R. O'BRIEN,** and C.D. WARRICK**

This is a preprint of a paper submitted for publication
in *Nuclear Fusion.*

Work supported by
U.S. Department of Energy
Contract DE-AC03-94SF20282
via Raytheon/Ebasco Subcontract ITER–4002
and by Contract W–7405–ENG–48

*Lawrence Livermore National Laboratory
**UKAEA/EURATOM Fusion Association

GENERAL ATOMICS PROJECT 3994
MARCH 1996

Electron Cyclotron Heating and Current Drive in ITER*

R.W. Harvey,† W.M. Nevins,‡ G.R. Smith,‡ B. Lloyd,♯
M.R. O'Brien,♯ and C.D. Warrick♯
General Atomics
San Diego, California 92186-9784, U.S.A.

Abstract

Electron cyclotron (EC) power has technological and physics advantages for heating and current drive (CD) in a tokamak reactor, and advances in source development make it credible for applications in the International Thermonuclear Experimental Reactor (ITER). Strong single pass absorption makes heating to ignition in ITER particularly simple. At densities to $3.6 \cdot 10^{20}$ m^{-3}, with Ohmic temperatures and wave frequency 170 GHz, heating in the plasma core is readily obtained. For outside launch of ordinary mode (O–mode) near the fundamental electron cyclotron frequency, the optimized EC current drive (ECCD) efficiency ($\langle n \rangle IR/P$) shows a linear temperature scaling at temperatures up to ~ 15 keV. For temperatures above 30 keV, the efficiency saturates at approximately $0.3 \cdot 10^{20}$ A/(m^{2}W) for a frequency of 220 GHz in an ITER target plasma with toroidal field of 6 T, due primarily to harmonic overlap [G.R. Smith *et al.*, Phys. Fluids **30** 3633 (1987)] and to a lesser extent due to limitations arising from relativistic effects [N.J. Fisch, Phys. Rev. A **24** 3245 (1981)].

The same efficiency can also be obtained at 170 GHz for the same plasma equilibrium and q-profile except that the magnetic field is reduced to $(170/220) \times 6$ T $= 4.6$ T. The ECCD efficiencies are obtained with the comprehensive 3D, bounce-averaged Fokker-Planck codes CQL3D [R.W. Harvey and M.G. McCoy, Proc. IAEA TCM/ Advances in Simulation and Modeling in Thermonuclear Plasmas 1992, Montreal] and BANDIT3D [M.R. O'Brien, M. Cox, C.D. Warrick, and F.S. Zaitsev, *ibid.*].

*This is a report of work supported by U.S. Department of Energy Contract No. Contract No. DE-AC03-94SF20282 via Raytheon/Ebasco Subcontract ITER-GA-4002 and by Contract No. DE-AC03-89ER51114.
†Present address: CompX, Del Mar, California, U.S.A.
‡Lawrence Livermore National Laboratory, Livermore, California, U.S.A.
♯UKAEA Fusion, Culham, Abingdon, Oxon OX14 3DB, U.K. (UKAEA/EURATOM Fusion Association).

1. Introduction

Electron cyclotron (EC) waves can fulfill a variety of roles in the International Thermonuclear Experimental Reactor (ITER), for example start-up assist, heating to ignition, current drive (CD), and instability control. In the present paper, we report the results of extensive calculations to examine the heating and CD potential of electron cyclotron waves in ITER and to determine the optimum system parameters based on launch of ordinary mode (O–mode) waves from the outboard midplane of the tokamak at a frequency near the fundamental electron cyclotron frequency.

Electron cyclotron heating (ECH) is a particularly *robust* heating scheme since the physics of wave propagation and absorption is well understood, there is total absorption for all plasma parameters foreseen in ITER, there are no requirements on plasma edge control, no specific impurity generation problems are anticipated, and no antenna structures need to be placed near damaging environment of the plasma. Absorption can be strong and localized near the plasma center over a very wide range of density and temperature. In particular, for near perpendicular injection the plasma density has only a minor effect on the location of the plasma heating up to densities in the vicinity of the cutoff density, $n_e \approx 3.6 \times 10^{20}$ m^{-3} at 170 GHz.

The CD calculations reported here examine optimization of electron cyclotron current drive (ECCD) by varying the wave frequency and injection angle in an ITER, ignited, target plasma. The ECCD efficiency is reported in terms of $\langle\gamma\rangle = \langle n\rangle\, IR/P$ where $\langle n\rangle$ is line averaged electron density, I is the driven current, R is the major radius of the magnetic axis, and P is the injected rf power. This form for $\langle\gamma\rangle$ removes the major dependencies of efficiency on $\langle n\rangle$, which is a factor in the collisional slowing-down of the electrons carrying the driven current, and R, which compensates for the number of transits an electron makes before it becomes thermalized. The remaining major dependence of the efficiency, after optimization of frequency and launch angle, is on plasma temperature. For a 6 T plasma, the optimized efficiency shows linear temperature scaling up to 15 keV. For temperatures above 30 keV and toroidal field of 6 T, the optimized efficiency saturates at approximately

$$\langle\gamma\rangle = 0.3 \times 10^{20} \text{ A/W-m}^2 \quad ,$$

for a 220 GHz beam launched from the plasma mid-plane with a launch angle ϕ = 40 deg in the toroidal direction, measured from the normal to the plasma surface.

Present high power gyrotrons operate at frequencies up to $\sim$ 170 GHz. At these lower, technologically more advantageous frequencies, the CD efficiency in full toroidal field simulations peaks at angles closer to the perpendicular, and is lower in magnitude. At f = 170 GHz and 6 T field, the peak efficiency is $\gamma \approx 0.19 \times 10^{20}$ A/W-m^2 at a launch angle of approximately 22 deg from perpendicular.

The ITER Joint Central Team has recommended 170 GHz as the frequency for the ITER EC heating and CD system. The high efficiency of 0.3×10^{20} A/W-m^2 can also be obtained at 170 GHz for the same plasma equilibrium except that the magnetic field is reduced to $(170/220) \times 6$ T = 4.6 T. Alternatively, a single gyrotron can be tuned to several frequencies by varying the magnetic field surrounding the microwave cavity. Recently, this has been accomplished with 118, 140, and 162 GHz at 750, 850, and 162 kW, respectively, for short pulses [1]. This flexible behavior promises new avenues for exploitation of gyrotron power, for heating and CD over a broad range of toroidal magnetic field. Also, at a given frequency, the injection angle can be varied vertically, so as to give additional radial variation of the deposition.

In the following, we briefly describe the computer codes used to obtain our results, discuss heating of Ohmic ITER target plasmas, discuss CD efficiency in ignited ITER target plasmas, and give results for the scaling of ECCD versus central electron temperature.

2. Description of CQL3D/BANDIT3D

The results reported here have been obtained with the CQL3D [2] and BANDIT3D [3] Fokker-Planck codes. The same results, to close approximation, have been independently obtained with these two codes for the 20 and 30 keV cases reported here; we also give results obtained for other conditions with one or the other of the two codes. The rf power densities are sufficiently low that the distribution function is observed to remain nearly Maxwellian [4]. The Fokker-Planck/quasilinear packages in these codes are the most complete models available. They incorporate the effects of momentum conserving electron-electron collisions which increase the CD efficiency by typically $\sim 20\%$ as compared to models which omit the current carried by the bulk electrons resulting from momentum transferred to them by collisions with the resonant electrons. These codes also take into account the actual variation of the magnetic field strength on a flux surface in calculating the effects of trapping on CD efficiency.

The codes are bounce-averaged, 2–D in momentum space, 1–D in the plasma radial variable, and are fully relativistic. Noncircular plasma geometry using actual ITER free-boundary equilibria and the finite angular width of the injected microwave beam are accounted for. Thus, the detailed effects of geometry on CD efficiency are taken into account. Note, however, that CQL3D presently assumes an up-down symmetric plasma, whereas this restriction is removed in BANDIT3D. Since the ITER equilibrium is not symmetric about the midplane, it is necessary with CQL3D to symmetrize the plasma by averaging the upper and lower elongation and triangularity before modeling the EC CD and heating. Both codes include a capability of modeling diffusive radial transport of the distribution function, but this effect is neglected here as it is small for ITER conditions.

The cold plasma dispersion relation has been used to obtain the ray paths along which the electron cyclotron energy travels. This dispersion relation is also used to obtain the parallel refractive index $n_{\parallel}$ along the ray. A relativistic dispersion tensor calculation [5] is then used to obtain the perpendicular refractive index $n_{\perp}$ and polarizations, which are required for calculation of the contribution to the quasilinear

diffusion coefficients due to each differential element along the ray. These contributions are bounce-averaged to obtain the net effect of the EC waves on the electron distribution. In addition, the local quasilinear operator due to each differential ray element is needed to calculate the damping of that ray element by the appropriate integration in momentum space over the electron distribution function. The second harmonic absorption, which overlaps parasitically [6] with the fundamental absorption is also accounted for.

The codes have been benchmarked by comparison of code results with analytical derivations of the neoclassical conductivity [7] (which verifies that the codes correctly handle collisions between passing and trapped particles) and with independent calculations of relativistic fundamental electron cyclotron absorption [5] (which validates the codes' quasilinear diffusion package and the treatment of the wave polarization). Comparisons with similar 3–D Fokker-Planck codes for a DIII–D experimental situation which was particularly sensitive to several competing effects such as trapping, tail formation, and dc electric field/EC synergy, showed good agreement amongst the codes [8].

3. Heating

A single null x–point configuration with elongation $\kappa \sim 1.55$ was utilized in the calculations, the equilibrium employed corresponding to a total plasma current of 24 MA. The magnetic axis is at a major radius of 8.2 m. (For CQL3D, the equilibria are up-down symmetrized about the vertical height of the magnetic axis, starting from an ITER/Engineering Design Activity (EDA) equilibria after Bulmer [9]. The magnetic field is varied by scaling the toroidal and poloidal fields, maintaining the q-profile.) Various values of toroidal magnetic field B_ϕ were assumed. In all cases, the values of B_ϕ quoted below correspond to the toroidal magnetic field at the nominal major radius $R_0 = 7.7$ m. Electron temperature and density profiles were of the form

$$T_\mathrm{e} = (T_\mathrm{eo} - T_\mathrm{ea}) \left(1 - r^2/a^2\right) + T_\mathrm{ea} \quad , \tag{1}$$

and

$$n_\mathrm{e} = (n_\mathrm{eo} - n_\mathrm{ea}) \left(1 - r^2/a^2\right)^{0.26} + n_\mathrm{ea} \quad , \tag{2}$$

respectively. An edge temperature $T_\mathrm{ea} = 0.5$ keV and an edge density $n_\mathrm{ea} = 0.8 \times 10^{20}$ m^{-3} were generally assumed. Calculations were carried out for various central electron temperatures T_eo but except where explicitly stated otherwise a central density of $n_\mathrm{eo} = 1.4 \times 10^{20}$ m^{-3} was assumed. For such a flat density profile with high edge density the average density (line-averaged or volume averaged) lies close to the central value. A flat Z_eff profile was assumed with $Z_\mathrm{eff} = 2$.

The most suitable scheme for both heating and CD in ITER utilizes low-field-side (LFS) injection of the ordinary mode (O–mode) with absorption primarily at the fundamental resonance. For the heating calculations described here, a cone of rays with Gaussian power distribution and half-angle 3 deg was launched from the outboard plasma midplane. The direction of launch is indicated by specification of the toroidal (ϕ) and poloidal (θ) launch angles, both measured with respect to the major radius vector. In calculating CD efficiencies the synergistic effect of the inductive dc electric field is small and therefore was ignored. Similarly, for the parameters employed in this study, fast electron transport has an insignificant effect on the results and was therefore neglected.

Operation at 160 GHz with perpendicular launch ($\phi = 0$ deg, $\theta = 0$ deg) allows core heating in ITER up to central densities $> 3 \times 10^{20}$ m^{-3}. Very strong localized absorption is observed even in the initial Ohmic phase of an ITER discharge. For example, at $T_{\rm eo} = 5$ keV ($T_{\rm ea} = 0.5$ keV) and $n_{\rm eo} = 3 \times 10^{19}$ m^{-3} ($n_{\rm ea} = 1 \times 10^{19}$ m^{-3}) the optical depth is ~ 30 indicating complete single pass absorption (Fig. 1) with the power absorbed inside $r/a \sim 0.1$ (*i.e.,* inside the flux surface which intersects the plasma midplane at $r/a = 0.1$). The optical depth increases to ~ 300 for parameters appropriate to the ignited phase (Fig. 2), *i.e.,* $T_{\rm eo} = 20$ keV ($T_{\rm ea} = 0.5$ keV) and $n_{\rm eo} = 1.4 \times 10^{20}$ m^{-3} ($n_{\rm ea} = 8 \times 10^{19}$ m^{-3}). Thus strong heating of the core can be maintained throughout the density ramp-up and approach to ignition.

The location of the peak of the power absorption profile is plotted as a function of toroidal magnetic field in Fig. 3 for frequencies in the range 150 to 170 GHz and for two central temperatures appropriate to the ignited phase, namely $T_{\rm eo} = 20$ and 30 keV. It is seen that the location of the power deposition does not depend strongly on temperature. For perpendicular launch at $B_\phi = 6.0$ T, 160 GHz gives the most central absorption. Of course, in all cases, as the toroidal field is reduced, the absorption moves further to the high-field-side of the magnetic axis. However, in this case, central absorption can be recovered by imposing a toroidal launch angle to give a significant Doppler shift which in turn leads to significant non-inductive current generation as discussed below. A significant second harmonic absorption peak can develop in situations as discussed in the following paragraph.

Because of the high electron temperature expected in ITER, downshifted ($\omega < 2\,\omega_{\rm c}$) second harmonic absorption, which can lead to a broadened power deposition profile, can be significant. Here, ω is wave frequency in radians per second, $\omega_{\rm c}$ is the local radian (rest mass) electron gyrofrequency. At the nominal operating field, namely $B_\phi \sim 6.0$ T at major radius $R \sim 7.7$ m, second harmonic absorption is negligible for frequencies in the range 150 to 170 GHz (perpendicular launch) even at central temperatures up to 30 keV, but soon becomes significant if B_ϕ is reduced, especially at 170 GHz (Fig. 4). Also note that the $T_{\rm e}$ dependence is strong. The second harmonic fraction of power absorption increases from 10% to 90% as $T_{\rm e}$ is raised from 20 to 30 keV, for 170 GHz at 5 T. However, second harmonic absorption remains low if the toroidal launch angle is slightly increased as B_ϕ is reduced. This will be explored in a future work.

Because of the cyclotron resonant nature of the heating scheme, it is sometimes mistakenly assumed that one has little control over the heating location, which is determined by the magnetic field and the chosen operating frequency. In fact, effective control of the heating zone at fixed magnetic field and frequency is possible by variation of the poloidal launch angle. This is illustrated in Fig. 5 where imposition of a poloidal launch angle of 27 deg is seen to move the heating zone out to $r/a \sim 0.4$ whilst maintaining very localized power deposition. In this example $f = 160$ GHz, $B_\phi = 6.0$ T, $T_{\rm eo} = 20$ keV ($T_{\rm ea} = 0.5$ keV) and $n_{\rm eo} = 1.4 \times 10^{20}$ m^{-3} ($n_{\rm ea} = 8 \times 10^{19}$ m^{-3}). The resonant magnetic field is illustrated by a solid line in Fig. 5(a). The distortion from a vertical line, which would correspond to the resonance in a purely toroidal vacuum field, arises because of the finite poloidal field and the influence of plasma diamagnetism.

In the following sections ECCD will be examined as a function of launch angle. It is therefore interesting to consider the variation of EC absorption versus launch angle for ITER Ohmic plasmas, to determine if the launch configurations appropriate for CD will also give sufficient absorption for ignition heating.

We investigate the dependence of the single-pass EC absorption on launch angle in two Ohmic target plasmas. Two plasma densities were considered for the Ohmic target plasmas with volume average $\langle n_{\rm e} \rangle_{\rm v} = 0.25 \times 10^{20}$ m^{-3} and 0.5×10^{20} m^{-3} (corresponding to $n_{\rm eo} = 0.275 \times 10^{20}$ m^{-3} and 0.55×10^{20} m^{-3}, respectively). The corresponding temperatures were computed assuming that the confinement was described by ITER89 L–mode scaling (retaining the Ohmic heating power in the computation of the confinement time as per recent results in Alcator C–Mod). This yielded central electron temperatures of $T_{\rm eo} = 13$ and 6.1 keV, respectively.

The projected single-pass absorption is shown versus launch angle in Fig. 6. We see that there is essentially full single-pass absorption for 170 GHz waves launched into Ohmic target plasmas for all launch angles below 40 deg. However, the radial location in the peak of the absorption is also a function of launch angle, as shown in Fig. 7. (r/a is the square root of toroidal flux within a flux surface, normalized to 1.0 at the plasma edge.)

The radial width of the power absorption varies between 10% and 20% of the plasma minor radius. Hence, deposition of EC power at the magnetic axis in full toroidal field scenarios would require a launch angle of 20 deg or less. However, results from DIII–D and T–10 on ECRF heating indicate that the effectiveness of ECRF

for plasma heating is only weakly dependent on the location of power absorption. Hence, launch angles as high as 35 deg should be acceptable in that they will provide excellent single-pass absorption and power deposition within the inner half of the plasma measured by radius (or inner quarter measured by volume).

4. Current Drive

ECCD was modeled in a 24 MA reference ITER/EDA discharge, using a plasma configuration after Bulmer [10]. (In general, the results will depend strongly on the local magnetic field strength although, since the poloidal field is fairly unimportant in the total field, there will only be weak dependence of the results on plasma current.) The toroidal magnetic field is 6.0 T at $R = 7.7$ m, and the magnetic axis is at $R = 8.43$ m. The plasma has a volume averaged density of 1.54×10^{20} m^{-3} with a very flat density profile of the form $n_e = n_{eo}(1 - \rho^2)^{0.1}$, and a peaked temperature profile of the form $T_e \sim (1-\rho^2)^2$. A microwave beam with a divergence of 10 deg (full width) was modeled by a bundle of 18 rays. The beam was launched in the plasma midplane at $R = 11.2$ m. The angle between the initial wave vector and the normal to the flux surface ϕ was varied between 5 to 50 deg in the toroidal direction, and the applied frequency was varied between 160 and 240 GHz.

The results of our survey of CD in target plasmas with $T_{eo} = 20$ and 30 keV are shown in Fig. 8(a) and (b). The CD efficiency depends strongly on both the EC wave frequency and on the launch angle ϕ. For each EC wave frequency there is an optimal launch angle ϕ_{max} at which the CD figure-of-merit has its maximum value $\langle\gamma\rangle_{max}$. At these elevated temperatures, the dependence on temperature is weak, as will be elaborated in the following section.

Figure 9 shows that the efficiency maximized over launch angle $\langle\gamma\rangle_{max}$ increases by a factor of two as the EC wave frequency is increased from 160 to 220 GHz, and then abruptly decreases at higher frequency. The corresponding optimal launch angles ϕ_{max}, shown in Fig. 10, are obtained for each EC wave frequency by fitting a parabola to the three largest values of $\langle\gamma\rangle$ at each frequency shown in Fig. 8(a) and (b). Note that the maximum in $\langle\gamma\rangle$ versus ϕ is rather broad, so that the CD figure-of-merit will be reduced by less than 10% if the center of the microwave beam is aimed to within 5 deg of the optimal launch angles shown in Fig. 10.

We note that at each EC wave frequency launched at the optimal launch angle the maximum in the driven current profile occurs at a plasma radius of less than $r/a = 0.2$ (see Fig. 11).

The variation of efficiency with frequency, launch angle, and radial location reflects a complex interplay between the increase in the frequency upshift at the location of wave absorption, that is increase in ω/ω_c (which results in a corresponding increase in the energy of the resonant electrons, leading to an increase in the CD figure-of-merit), parasitic second-harmonic absorption (which generally increases with increasing ECH frequency and electron temperature, and leads to a reduction in the CD figure-of-merit), and the radial location of the microwave power absorption (giving electron trapping effects, which increase rapidly as the absorption moves away from the magnetic axis and can greatly reduce the CD efficiency).

In general terms, these effects are largely controlled by the relativistic resonance condition

$$\omega - k_{\parallel} v_{\parallel} - n\,\omega_c/\gamma = 0 \quad , \tag{3}$$

where n is the harmonic of the cyclotron interaction, $k_{\parallel}$ is the wavenumber, $v_{\parallel}$ is the parallel velocity of the resonant electron, and γ (in this context) is the relativistic factor. This is an equation for an ellipse in momentum-per-mass-space: with $u_{\parallel} \equiv p_{\parallel}/m_e = \gamma\, v_{\parallel}$, $u_{\perp} \equiv p_{\perp}/m_e$, and parallel refractive index $n_{\parallel} = k_{\parallel} c/\omega$, then

$$\left(u_{\parallel} - u_{\parallel o}\right)^2 + u_{\perp}^2 \Big/ \left(1 - n_{\parallel}^2\right) = u_o^2 \quad , \tag{4}$$

where

$$\frac{u_{\parallel o}}{c} = \frac{n\omega_c}{\omega} \cdot \frac{n_{\parallel}}{1 - n_{\parallel}^2} \quad , \tag{5}$$

$$\frac{u_o^2}{c^2} = \left\{ \left(\frac{n\,\omega_c}{\omega}\right)^2 - \left(1 - n_{\parallel}^2\right) \right\} \Big/ \left(1 - n_{\parallel}^2\right)^2 \quad . \tag{6}$$

It is instructive to consider the variation of the resonance ellipse as a function of major radius along a ray, for example. In Fig. 12, the minimum (u_{min}/c) and maximum (u_{max}/c) values of u/c [$= (u_{\parallel}^2 + u_{\perp}^2)^{1/2}/c$] on the resonance ellipses are plotted as a function of ω/ω_c (or R/R_c at constant ω, taking the B field to vary as R^{-1}; R_c is the major radius of cyclotron resonance for frequency ω), for $n_{\parallel} = n_{\parallel o}\, R_c/R$ (choosing this on the basis that $n_{\parallel} \approx n_{\phi}$ and $n_{\phi} R$ is constant due to toroidal symmetry, where n_{ϕ} is the component of the refractive index in the toroidal direction). The

refractive index at the resonance surface corresponds to 50 deg from perpendicular. As an example, application of the curves in Fig. 12 to the specific equilibrium and launch location used for the CD results [10], 160 GHz is at cyclotron resonance with electrons at the magnetic axis, that is $R_{\rm mag}/R_{\rm c,160} = 1$. The horizontal axis value corresponding to EC frequency 200 GHz and R at the magnetic axis ($R = 8.43$ m) is marked by $R_{\rm mag}/R_{\rm c,200}$, and the value of R at the launch point just outside the plasma by $R_{\rm launch}/R_{\rm c,200}$. Higher frequency would move $R_{\rm launch}/R_{\rm c}$ to higher values of the horizontal coordinate, indicating a lower value for $|u_{\rm min}/c|$ for the second harmonic, thus greater second harmonic absorption.

Due to relativistic effects, as EC energy propagates along the rays from the outboard side of the tokamak there is no fundamental ($n = 1$) harmonic absorption, that is, no solution for real $v_{\parallel}$ to the resonance equation [Eqs. (3) or (4)] until the point where

$$\left(\frac{\omega_{\rm c}}{\omega}\right)^2 = 1 - n^2_{\parallel {\rm pp}} \quad , \tag{7}$$

where $\omega_{\rm c}$ is the local cyclotron frequency, ω is the wave frequency, and $n_{\parallel {\rm pp}}$ the local refractive index at this "pinch point." This is the zero of Eq. (6), and this point is indicated by "pp" in Fig. 12. In the outboard launch cases studied here, and at densities significantly below the cutoff densities such that $n_{\parallel}$ remains close to its vacuum value, the magnitude of $n_{\parallel}$ thus increases toward 1.0 as the launch angle increases, whereas $\omega_{\rm c}/\omega$ increases along the ray toward 1 at the cyclotron layer $\omega = \omega_{\rm c}$. At the pinch point, which is reached outboard of the cyclotron layer and is where the relativistic resonance condition along the ray can first become satisfied, the energy of resonant particles is $E_{\rm pp} = (\gamma_{\rm pp} - 1)\, mc^2$, with

$$\gamma^2_{\rm pp} = \frac{1}{1 - n^2_{\parallel {\rm pp}}} \quad . \tag{8}$$

The major radius of the pinch point $R_{\rm pp}$ relative to that of the resonance $\omega = \omega_{\rm c}$-layer $R_{\rm c}$ is from Eq. (7)

$$\left(\frac{R_{\rm pp}}{R_{\rm c}}\right)^2 = \frac{1}{1 - n^2_{\parallel {\rm pp}}} \quad , \tag{9}$$

where the magnetic field variation in ω_c has been approximated as R^{-1}. Thus as the launch angle is increased from perpendicular, $n_{\parallel_{pp}}$, γ_{pp}, and the resonant energy all increase. But also the major radius R_{pp} of the pinch point increases. When R_{pp} becomes greater than the major radius at the magnetic axis R_{mag}, toroidal trapping becomes a factor which tends to decrease the CD efficiency. Also, the peaking of the temperature profile at the magnetic axis favors maximization of $\langle\gamma\rangle$ near the magnetic axis. Thus as the frequency increases, since R_c becomes smaller, $n_\parallel$ can be increased to give greater energy E_{pp} and hence greater efficiency, still keeping R_{pp} near R_{mag}. The parasitic loss of EC power due to the second harmonic overlap [6] intervenes in the process of higher frequency and higher launch angle leading to higher CD efficiency. This overlap is the major factor which prevents attainment of even greater efficiency. Interestingly, the second harmonic generally contributes a small *positive* component to the CD [11].

The CD results in Fig. 8 can now be further understood with the help of the results from Fig. 13(a) and (b). Figure 13 gives the CD figure-of-merit $\langle\gamma\rangle$, the radial location of the peak in the driven current profile $(r/a)_{max}$, and the fractional absorption due to the second harmonic resonance, for frequency 170 GHz [Fig. 13(a)] and 200 GHz [Fig. 13(b)], for the $T_{eo} = 30$ keV case, as a function of EC launch angle ϕ. The main point to notice here is that in both cases the maximum of the CD efficiency occurs at a point only slightly outboard of the magnetic axis, at $(r/a) \sim 0.2$. At 170 GHz [Fig. 13(a)] the second harmonic damping is $\lesssim 20\%$, but at 200 GHz [Fig. 13(b)] the second harmonic damping is becoming an important factor, pushing the peak of the CD efficiency further outward from the magnetic axis. At 240 GHz, the parasitic second harmonic absorption dominates at all injection angles.

An additional consideration is that at a launch angle of 45 deg, the rays just graze the magnetic axis. At higher angles, the rays only pass outside of the magnetic axis, where trapping effects reduce the CD efficiency. This also pulls down the CD efficiency at angles greater than 45 deg.

In summary of this section, a CD efficiency up to $\langle\gamma\rangle = 0.26\,(0.30) \cdot 10^{20}$ A/(W·m^2) is obtained at frequency 220 GHz for a full magnetic field ITER plasma with central temperature $T_{eo} = 20\,(30)$ keV. Parasitic second harmonic overlap prevents attainment of greater efficiency at even larger frequency.

We expect the CD efficiency to vary with EC wave frequency mainly as a function of the ratio between the wave frequency and the electron cyclotron frequency at the magnetic axis. Hence, if the B-field of the target plasma is reduced by the amount $(170/220) \approx 0.77$, the electron cyclotron CD efficiency at 170 GHz should be nearly equal to that obtained at 220 GHz in a full-field target plasma. We investigate this by comparing the CD figure-of-merit computed for 220 GHz waves injected into a 6 T target plasma with a central temperature, $T_{\rm eo} = 30$ keV, with that obtained when injecting 170 GHz waves into a target plasma in which B_0 is reduced to $(170/220) \times 6$ T $= 4.636$ T. The results of this survey are shown in Fig. 14. We see that the reduction in the peak CD figure-of-merit is less than 10%, with $\langle\gamma\rangle$ peaking at 0.28×10^{20} A/W-m^2 for 170 GHz into the $B_0 = 4.636$ T target plasma, versus $\langle\gamma\rangle = 0.30 \times 10^{20}$ A/W-m^2 for 220 GHz into the $B_0 = 6$ T target plasma. The slight reduction in efficiency seems to be related to a reduction in opacity which occurs for the lower frequency/B-field combination. This reduction in opacity results in the absorption being on slightly less energetic electrons with slightly less CD capacity. Thus the present technically accessible source frequency 170 GHz can give almost as high CD efficiency as 220 GHz, if the B-field is reduced.

5. Optimized Current Drive Efficiency Versus T_{eo}

Sets of runs have been performed at various temperatures, varying launch angles, and wave frequency, as in the previous 20/30 keV cases. At each temperature, results are obtained analogous to those shown in Fig. 8.

The peak (*i.e.,* optimized over frequency and launch angle) efficiencies $\langle\gamma\rangle_{\rm opt}$ obtained in each of these runs are presented in Fig. 15 as a function of $T_{\rm eo}$. Results are given for the ±5 deg divergence (10 deg full width) 18-ray cases such as in Fig. 8, as well as for single ray cases with the narrow $T_{\rm e}$-profile $\sim (1-\rho^2)^2$, and with a broader temperature profile, $T_{\rm eo} \sim (1-\rho^2)$. Also shown are experimental points which we will briefly discuss below.

The main feature is that the CD efficiency exhibits a saturation setting in above a central electron temperature of 20 to 30 keV. The major cause of the saturation is the second harmonic overlap. As the temperature increases, the resonant energy $E_{\rm pp}$ of the pinch point can be increased in accord with Eq. (8), still obtaining sufficient damping. The increasing resonant energy leads to greater CD efficiency, in accord with the Fisch-Boozer mechanism [12]. But the wave frequency must also be increased in accord with Eq. (9), to keep the pinch point near the plasma center. As the wave frequency is increased, the second harmonic overlap becomes more of a limiting factor. At $T_{\rm eo} = 30$ keV, the second harmonic absorption is a significant factor in degrading CD efficiency, as evidenced by the difference between the single ray results in the peaked $T_{\rm e}$-profile [$\sim (1-\rho^2)^2$], compared to the broader $T_{\rm e}$-profile $\sim (1-\rho^2)$. At 30 keV, second harmonic absorption is moving the peak of the CD efficiency off-axis [see Fig. 13(b)] into the region of trapping-reduction of the efficiency, giving the saturation of efficiency.

A secondary cause for saturation is relativistic effects [13]. The CD efficiency is a function of parallel resonance momentum-per-mass $u_\parallel$. For diffusion in $u_\perp$, the efficiency increases proportional to $u_\parallel^2$ at low velocity, but maximizes at $u_\parallel/c \approx 2$. [For $T_{\rm eo} \lesssim 75$ keV, see Fig. 2(b) of Ref. 13]. At $T_{\rm e} = 25$ keV, the efficiency at $u_\parallel/c = 1$ has achieved about 80% of its $u_\parallel/c = 2$-maximum (when there is a parallel component to the QL diffusion then this limit may be relaxed). The maximum CD efficiency which

we have obtained at 30 keV is near the absolute maximum consistent with relativistic limits for perpendicular diffusion (usually the case for EC, although this limitation may be relaxed in the "auto-resonant" case described by Kuyanov *et al.* [14], if cases can be found with both parallel diffusion and significant wave damping).

Experimental points have been included in Fig. 15 for comparison with the optimized value. The DIII–D results [15] and T–10 results [16] are for fixed launch angles and thus are not optimized over launch angle for the particular experimental conditions obtained, as can be easily done with the codes, but the results have been adjusted upward (from the experimental values represented by the open squares) to account for the quite flat density profile and low $Z_{\rm eff}$ assumed in the study here. (The experimental points used here are for situations of low loop voltage synergy with the ECCD [17].) Close agreement between the CQL3D code and the experiment is obtained [15,18]. Evidently the experimental efficiency improves with $T_{\rm e}$ but much higher temperature plasmas are required to achieve the full CD efficiencies that EC waves are capable of. Future work will focus on optimization of off-axis CD for profile control in advanced tokamak operations.

6. Conclusions

Central heating of Ohmic ITER plasmas is readily obtained with O–mode EC waves, over a broad range of launch angles. The CQL3D and BANDIT3D Fokker-Planck codes have been used to calculate the maximum CD efficiencies γ obtainable in ITER/ EDA for EC waves launched at the outer equatorial plane of the tokamak. At low temperature, the optimized efficiency $\langle\gamma\rangle_{\rm opt}$ scales approximately linearly with plasma temperature $T_{\rm eo}$. At 20 keV, onset of a saturation of $\langle\gamma\rangle_{\rm opt}$ was evident, and at 30 keV, the maximum efficiency is $0.3 \cdot 10^{20}$ A/(m^2·W). The optimal wave frequency in a full field ITER equilibrium at 30 keV is approximately 220 GHz at launch angle 40 deg from perpendicular in the toroidal direction. Approximately the same efficiency can be obtained at 170 GHz, if the plasma magnetic field is reduced in proportion to the frequency.

7. Acknowledgments

R.W.H. wishes to acknowledge contributions by Drs. Y.R. Lin-Liu and S.C. Chiu in verification of CQL3D.

This is a report of work supported by U.S. Department of Energy Contract No. DE-AC03-94SF20282 via Raytheon/Ebasco Subcontract ITER-4002 and Contract No. W-7405-ENG-48. Part of the work was jointly funded by the U.K. Department of Trade and Industry and by Euratom.

8. References

[1] THUMM, MANFRED, personal communication (1995).

[2] HARVEY, R.W., McCOY, M.G., in *Proc. IAEA TCM on Simulation and Modeling of Thermonuclear Plasma, Montreal, 1992* IAEA, Vienna, 1993) p. 489.

[3] O'BRIEN, M.R., COX, M., WARRICK, C.D., ZAITSEV, F.S., *ibid.*, p. 527.

[4] HARVEY, R.W., McCOY, M.G., KERBEL, G.D., Phys. Rev. Lett. **62** (1989) 462.

[5] MAZZUCATO, E., FIDONE, I., GRANATA, G., Phys. Fluids **30** (1987) 3745.

[6] SMITH, G.R., COHEN, R.H., MAU, T.K., Phys. Fluids **30** (1987) 3633.

[7] CONNOR, J.W., GRIMM, R.C., HASTIE, R.J., KEEPING, P.M., Nucl. Fusion **13** (1973) 211.

[8] WESTERHOF, E., in *Proc. 9th Joint Workshop on ECE and ECRH, Borrego Springs, 1995* (LOHR, J., Ed.), World Science Publishers, Singapore (1995) p. 3.

[9] BULMER, R.H., equilibrium 93046-3 "Start of Flat-top," personal communication (1993).

[10] BULMER, R.H., equilibrium 93046-2 "Start of Burn," personal communication (1993).

[11] LLOYD, B., O'BRIEN, M.R., WARRICK, C.D., in *Proc. 21st Euro. Conf. on Contr. Fusion and Plasma Heating, Montpellier, 1994* Vol. II, p. 1012.

[12] FISCH, N.J., BOOZER, A.H., Phys. Rev. Lett. **45** (1980) 1549.

[13] FISCH, N.J., Phys. Rev. A **26** (1981) 3245; KARNEY, C.F.F., FISCH, N.J., Phys. Fluids **28** (1985) 116.

[14] KUYANOV, A.Yu., SKOVORODA, A.A., TOKMAN, M.D., in *Proc. of European Physical Society Conference on Controlled Fusion and Plasma Physics, Bournemouth, 1995*, European Physical Society, Petit Lancy (1995) Vol. 1, p. 365.

[15] JAMES, R.A., *et al.*, Phys. Rev. A **45** (1992) 8723.

[16] ALIKAEV, V.V., *et al.*, Nucl. Fusion **32** (1992) 1811.

[17] HARVEY, R.W., FOREST, C.B., SAUTER, O., LOHR, J., LIN-LIU, Y.R., in *Radio Frequency Power In Plasmas* (Proc. 10th Top. Conf. on RF Power in Plasmas, Boston, 1993) (PORKOLAB, M., HOSEA, J., Eds.) AIP Conf. Proc. 289, American Institute of Physics, New York (1994) p. 169.

[18] JAMES, R.A., PETTY, C.C., HARVEY, R.W., in *Proc. Ninth Joint Workshop on Electron Cyclotron Emission and Electron Cyclotron Heating, Borrego Springs, 1995* (LOHR, J., Ed.), World Science Publishers, Singapore (1995) p. 76.

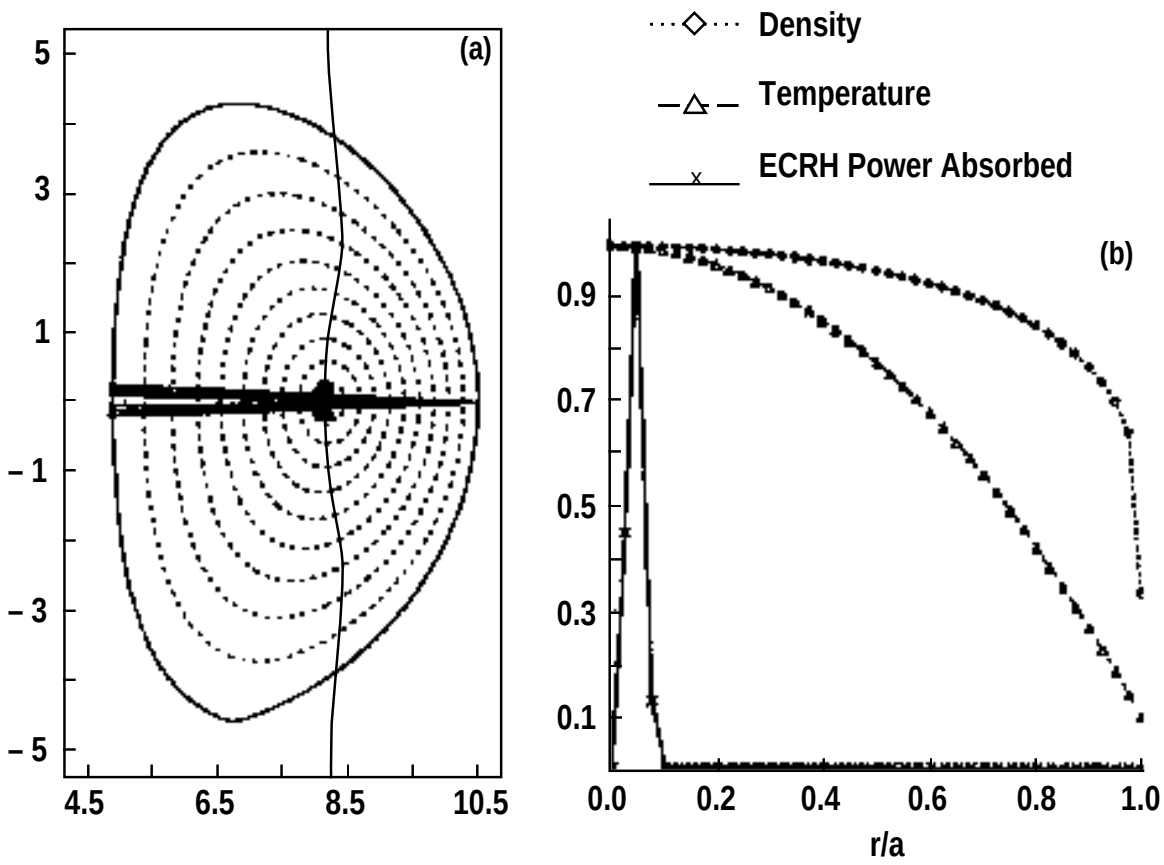

Fig 1. (a) Ray trajectories and (b) absorption profile for the initial Ohmic phase of an ITER discharge. The rays are launched radially. The ''x'' symbols along the ray trajectories in (a) [and in Figs. 2(a) and 5a)] indicate successive positions where power is reduced by 10% of the input power. Relative profiles of electron temperature and density are also shown in (b) and $T_e(0) = 5$ keV and $n_e(0) = 3 \times 10^{19}$ m^{-3}. The toroidal field is 6 T and the plasma current is 24 MA.

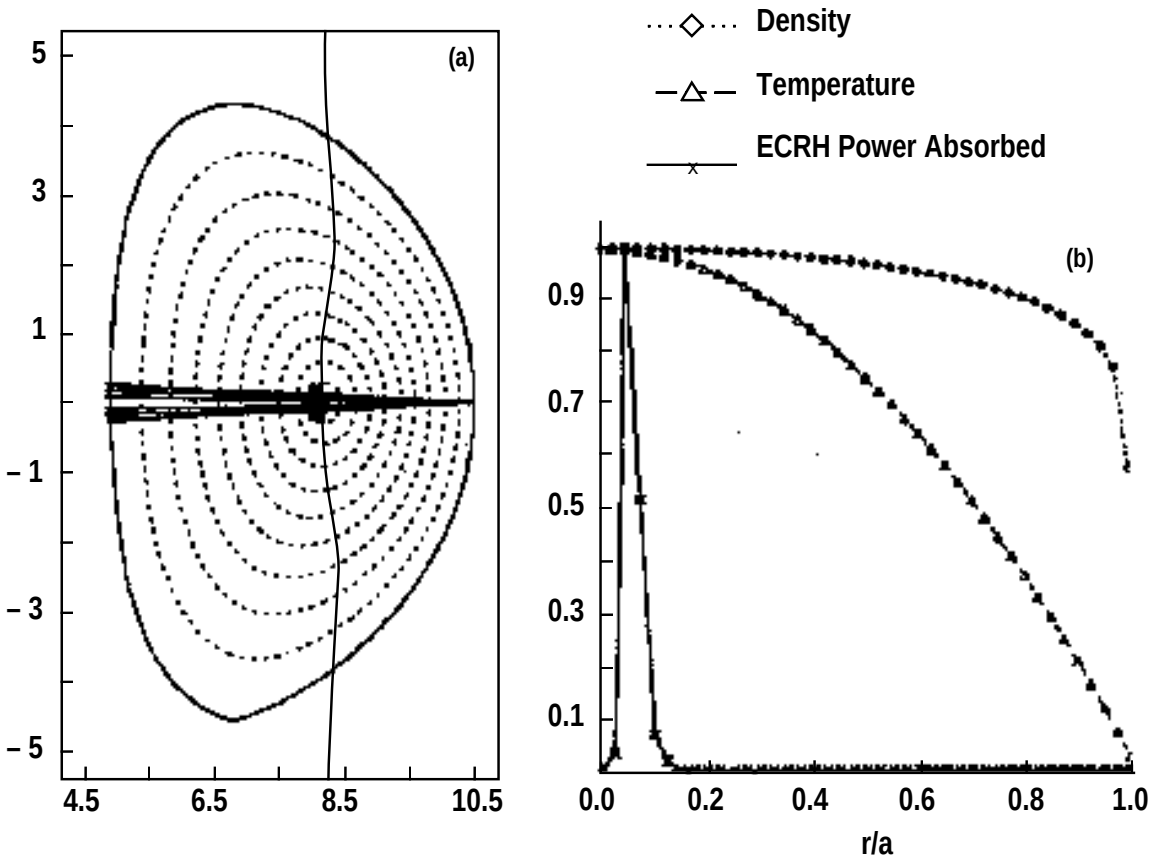

Fig. 2. Ray trajectories and absorption profile for the ignited phase of an ITER discharge, for radial launch of the rays. Here, $T_e(0) = 20$ keV and. $n_e(0) = 1.5 \times 10^{20}$ m^{-3}.

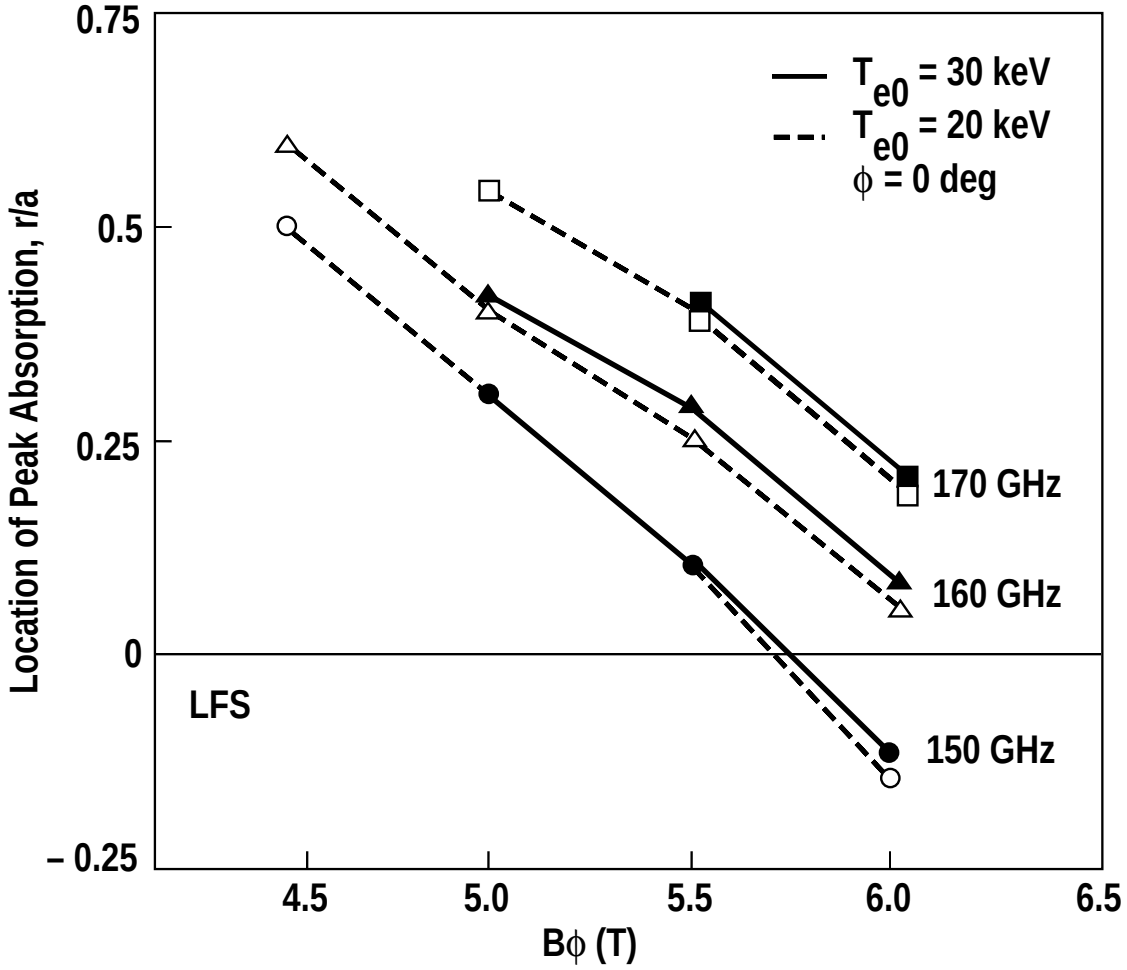

Fig. 3. Location of power deposition versus B_ϕ (evaluated at $R = 7.7$ m) for fundamental absorption (perpendicular launch).

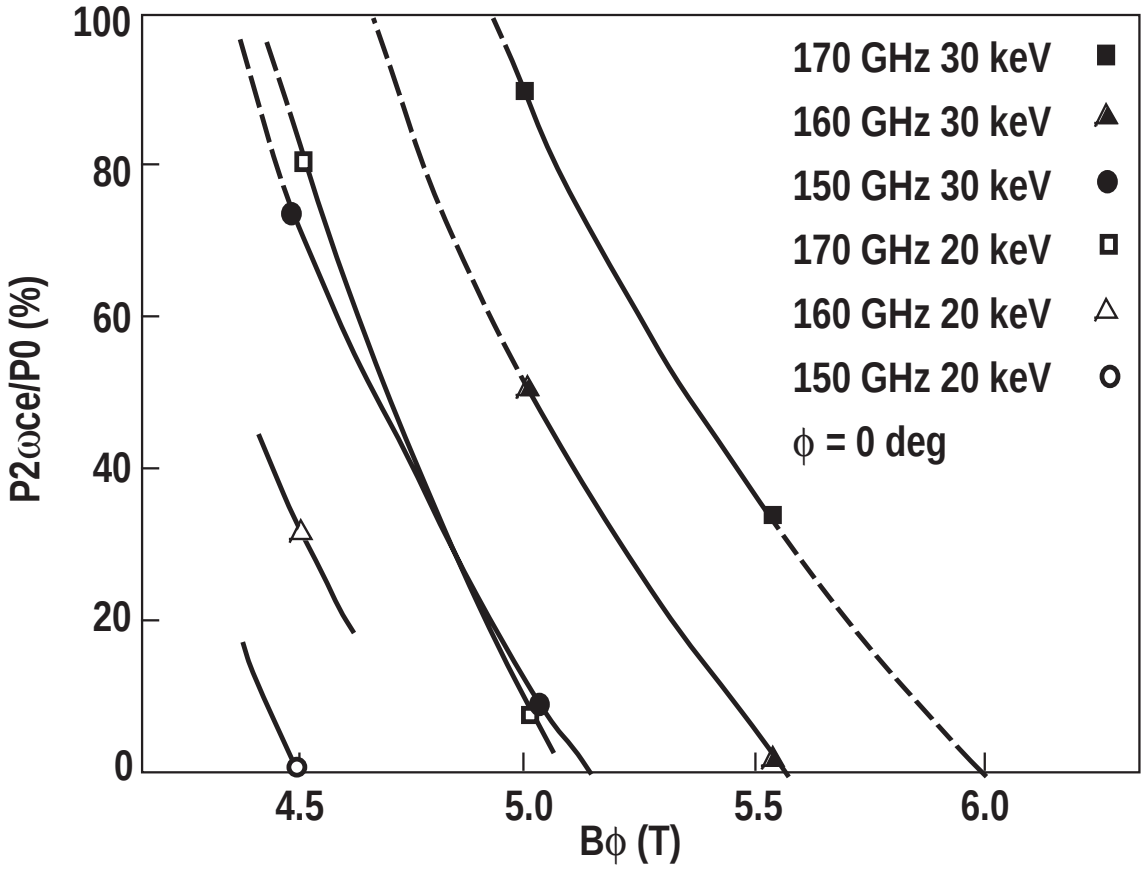

Fig. 4. Fraction of second harmonic absorption versus B_ϕ (evaluated at $R = 7.7$ m) for fundamental absorption (perpendicular launch).

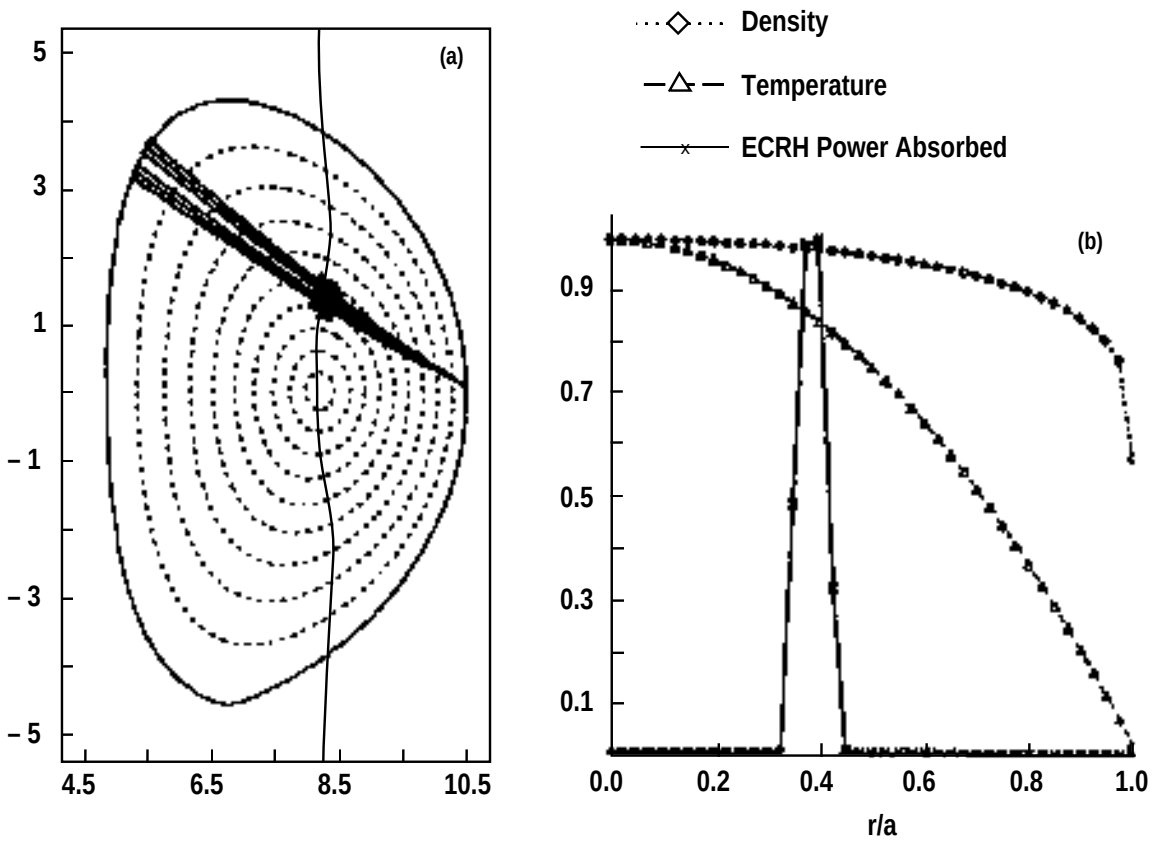

Fig. 5. Control of heating zone by variation of poloidal launch angle.

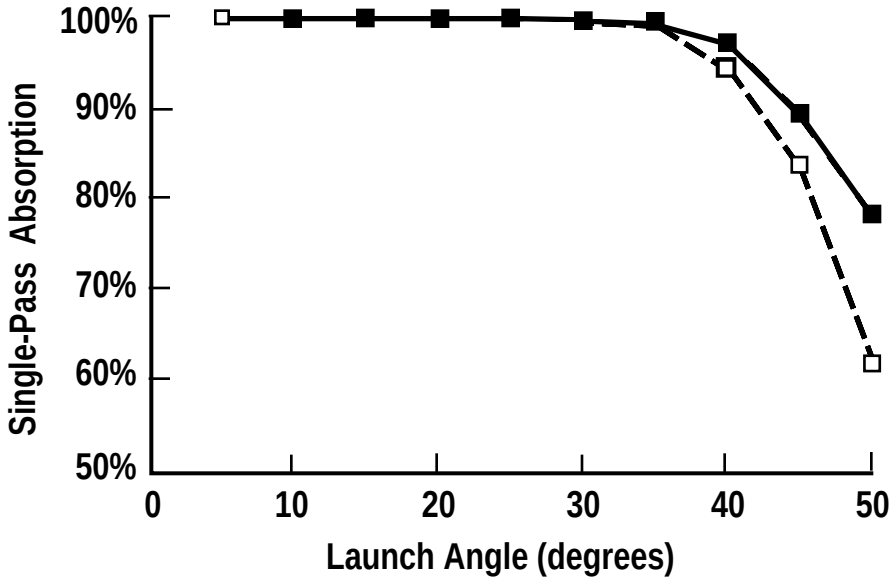

Fig. 6. Single pass absorption plotted versus launch angle for 170 GHz waves injected into a 24 MA target plasma with $\langle n_e \rangle = 0.25 \times 10^{20}$ m^{-3} and T_{e0} = 13 keV (solid line), or $\langle n_e \rangle = 0.5 \times 10^{20}$ m^{-3} and $T_{e0} = 6.1$ keV (dashed line).

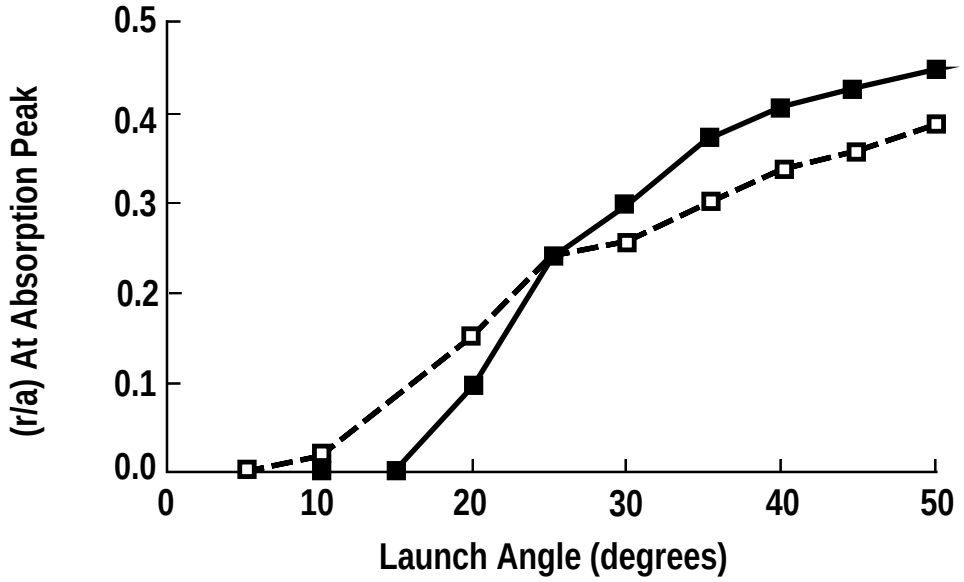

Fig. 7. Normalized radius r/a for the peak in the EC power absorption plotted versus launch angle for 170 GHz waves injected into a 24 MA target plasma with $\langle n_e \rangle = 0.25 \times 10^{20}$ m^{-3} and $T_{e0} = 13$ keV (solid line), or $\langle n_e \rangle = 0.5 \times 10^{20}$ m^{-3} and $T_{e0} = 6.1$ keV (dashed line).

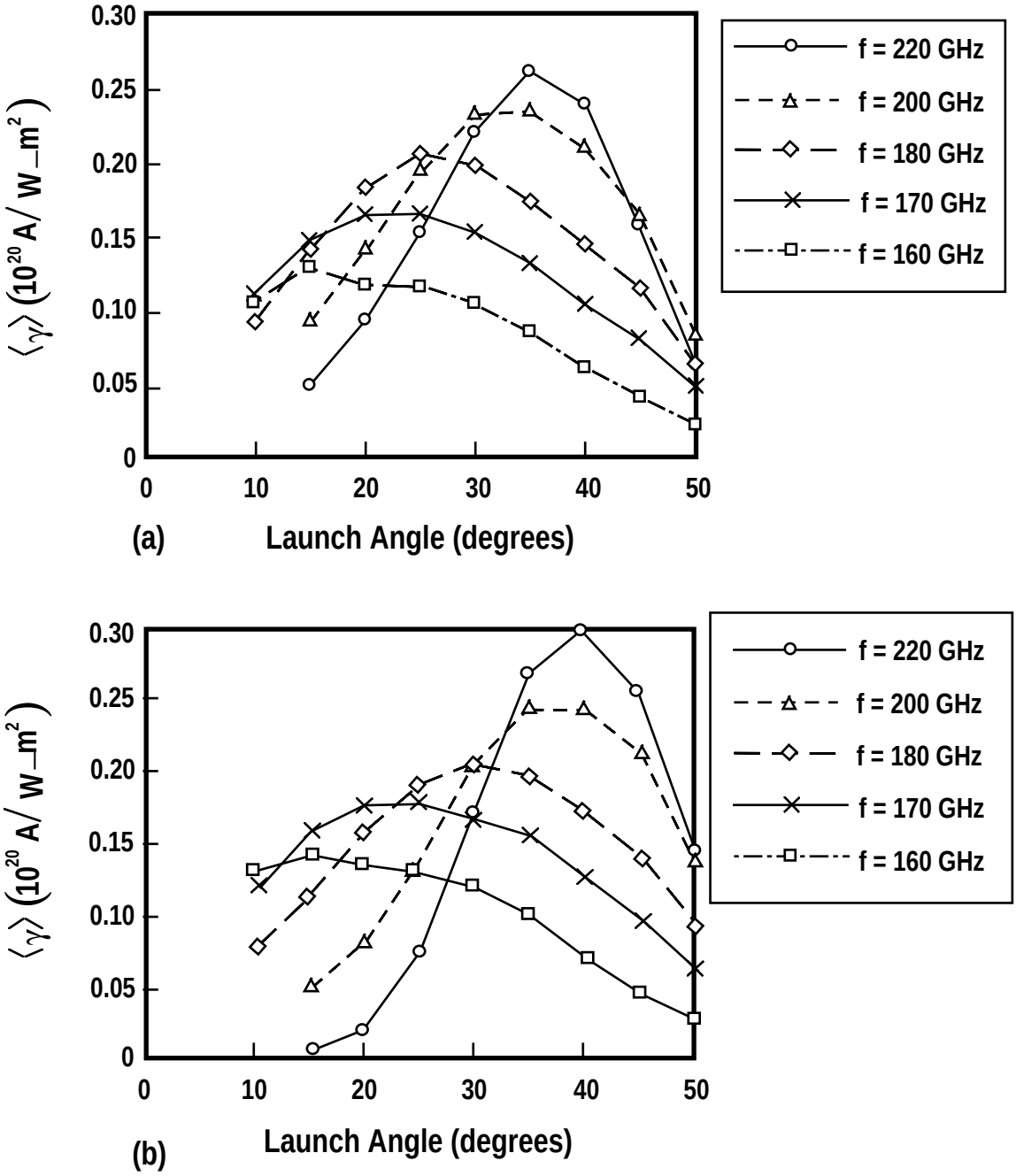

Fig. 8. CD figure-of-merit for a 24 MA target plasma with (a) $T_{e0} = 20$ keV and (b) $T_{e0} = 30$ keV. The figure-of-merit $\langle\gamma\rangle$ is plotted against launch angle ϕ for a variety of EC frequencies. The toroidal field is 6 T at $R = 7.7$ m and central density is 1.7×10^{20} m^{-3}.

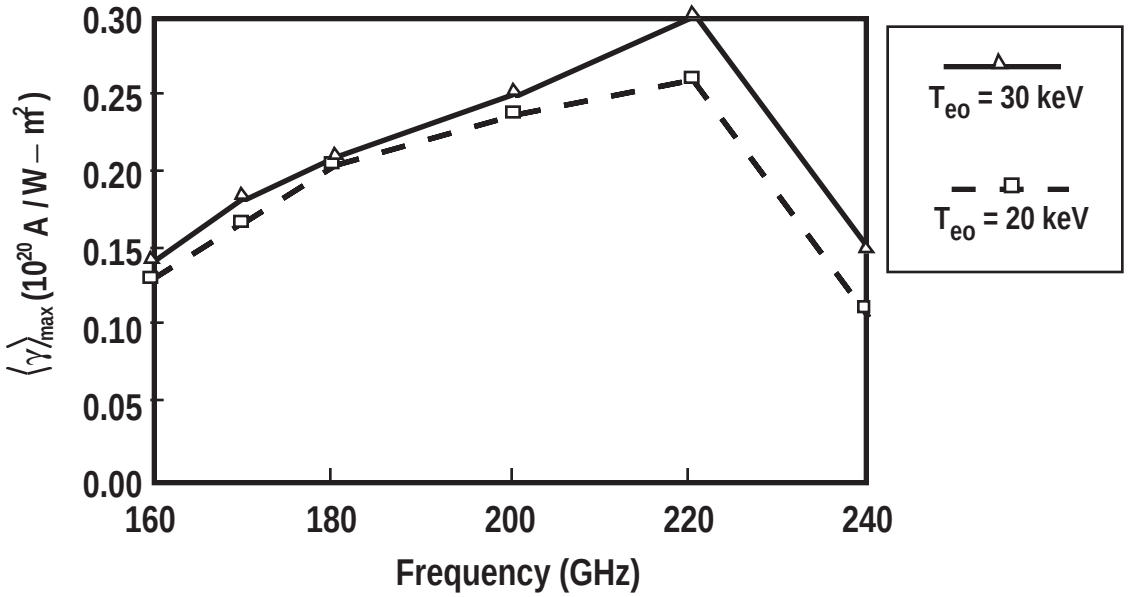

Fig. 9. CD figure-of-merit $\langle\gamma\rangle_{\max}$, maximized over launch angle, for 24 MA target plasmas with T_{e0} = 20 and 30 keV, plotted versus EC wave frequency.

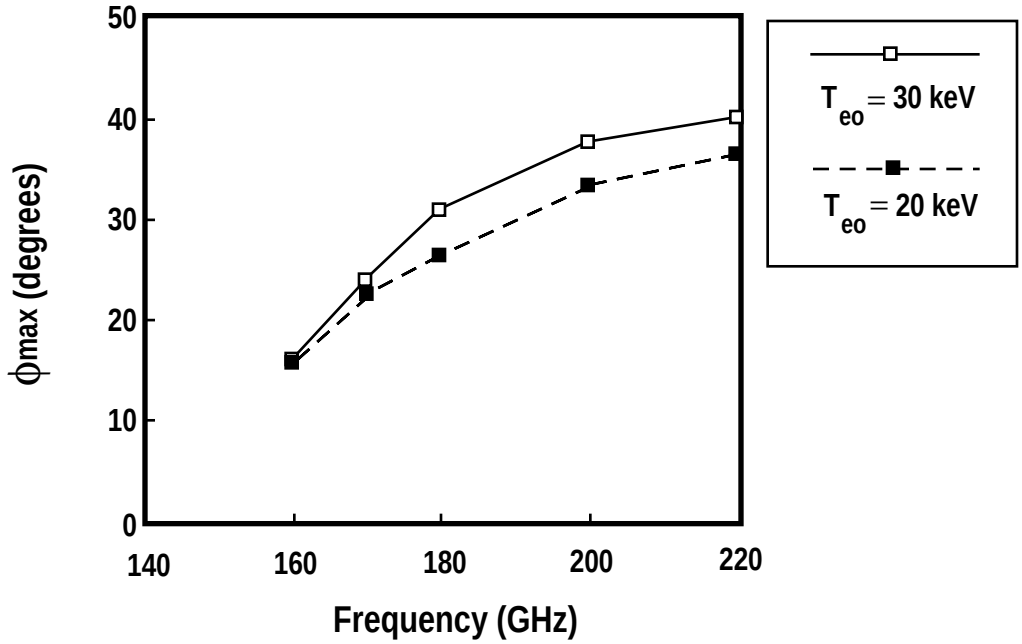

Fig. 10. Optimal launch angle $\phi_{\max}$ for 24 MA target plasmas with T_{e0} = 20 and 30 keV plotted versus EC wave frequency.

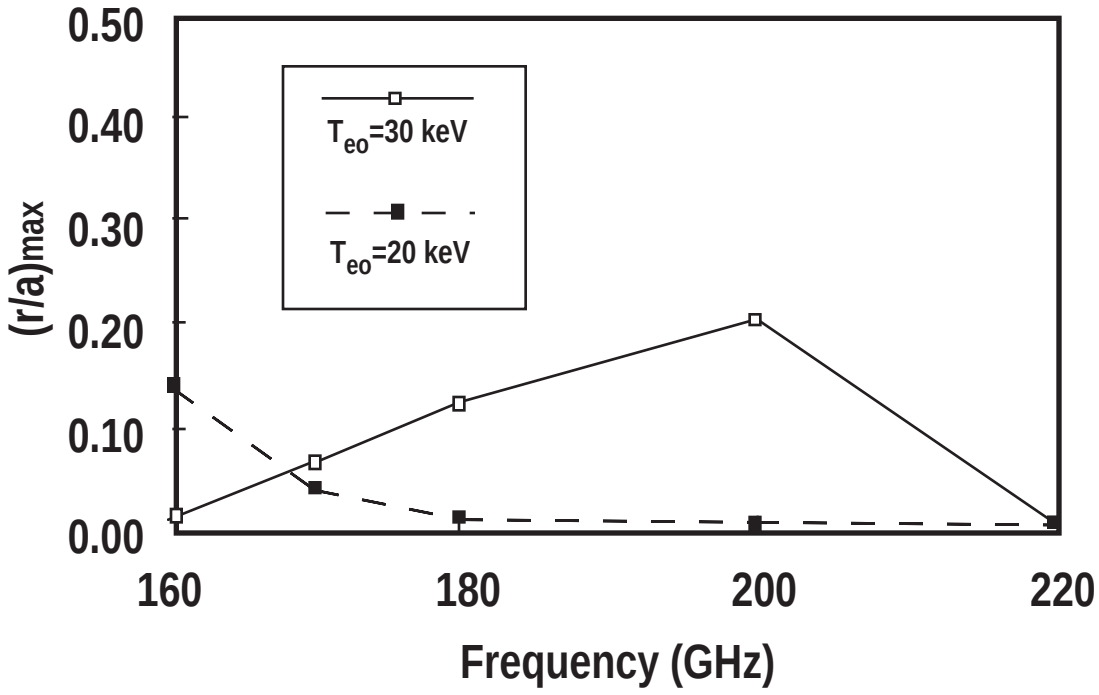

Fig. 11. Radial location of the maximum in the driven current (and the EC power absorption) $(r/a)_{\max}$ versus EC wave frequency. We evaluate $(r/a)_{\max}$ for waves launched at the angle $\phi_{\max}$ which optimizes the CD figure-of-merit. The data plotted here are from the same 24 MA target plasmas with $T_{e0} = 20$ and 30 keV used in producing the data shown in Fig. 8(a) and (b).

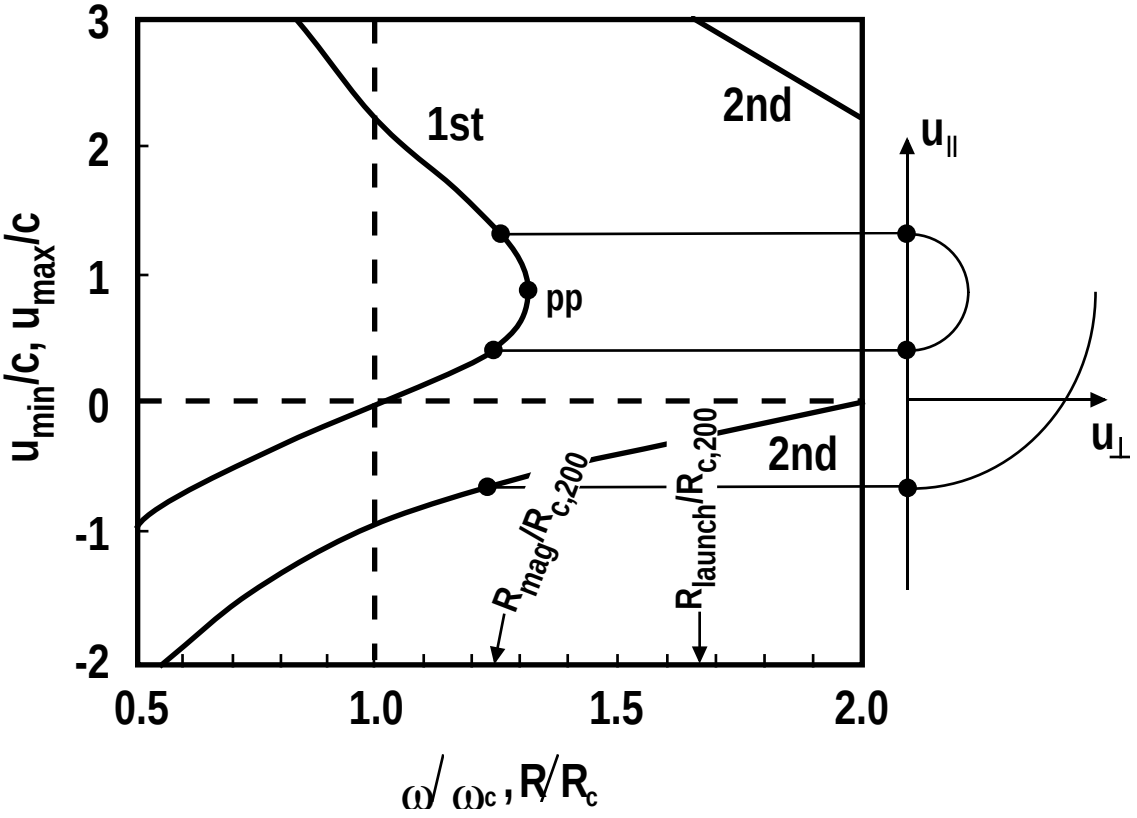

Fig. 12. The minimum and maximum momentum-per-mass for the first and second cyclotron harmonic interactions versus normalized frequency and normalized major radius. ω_c is cyclotron frequency assumed to vary at R^{-1}, R_c is major radius at which frequency $\omega = \omega_c$. $R_{c,200}$ is R_c at 200 GHz for an ITER/EDA plasma equilibrium.

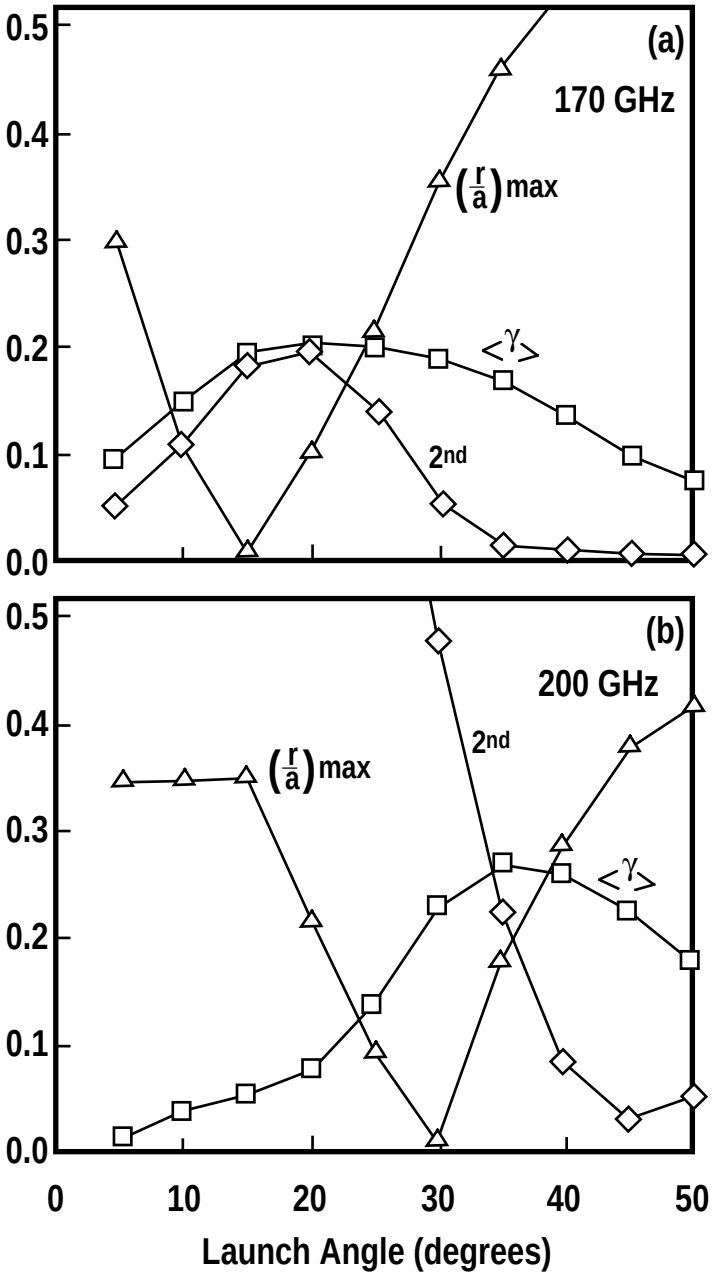

Fig. 13. (a) CD figure-of-merit $\langle\gamma\rangle$, radial location of the peak of the driven current profile $(r/a)_{\max}$, and the fractional absorption due to the second harmonic resonance (2nd) are plotted against launch angle ϕ. This is for 170 GHz radiation launched into the same 24 MA target plasmas at 30 keV as used in producing the data in Fig. 8(b). (b) Results at 200 GHz; otherwise the same as (a).

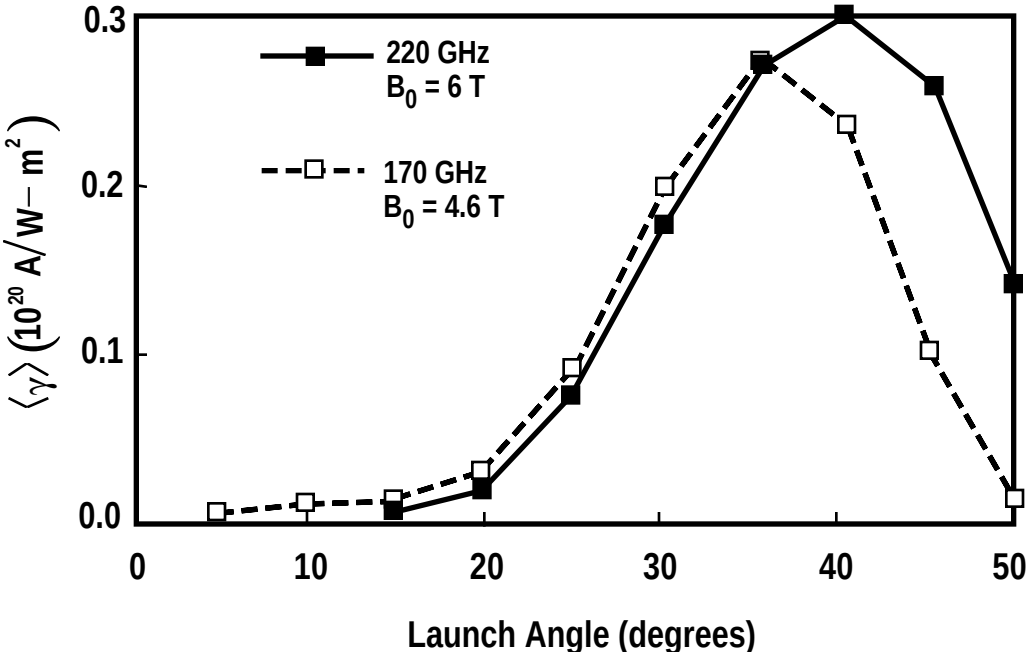

Fig. 14. The CD figure-of-merit $\langle\gamma\rangle$ for 220 GHz EC waves injected into a 6 T target plasma (solid line) and for 170 GHz waves injected into a 4.636 T target plasma (dashed line), as a function of launch angle. In both target plasmas, the temperature and density were held fixed at $T_{e0} = 30$ keV and $n_{e0} = 1.7 \times 10^{20} \backslash \text{m}^{-3}$.

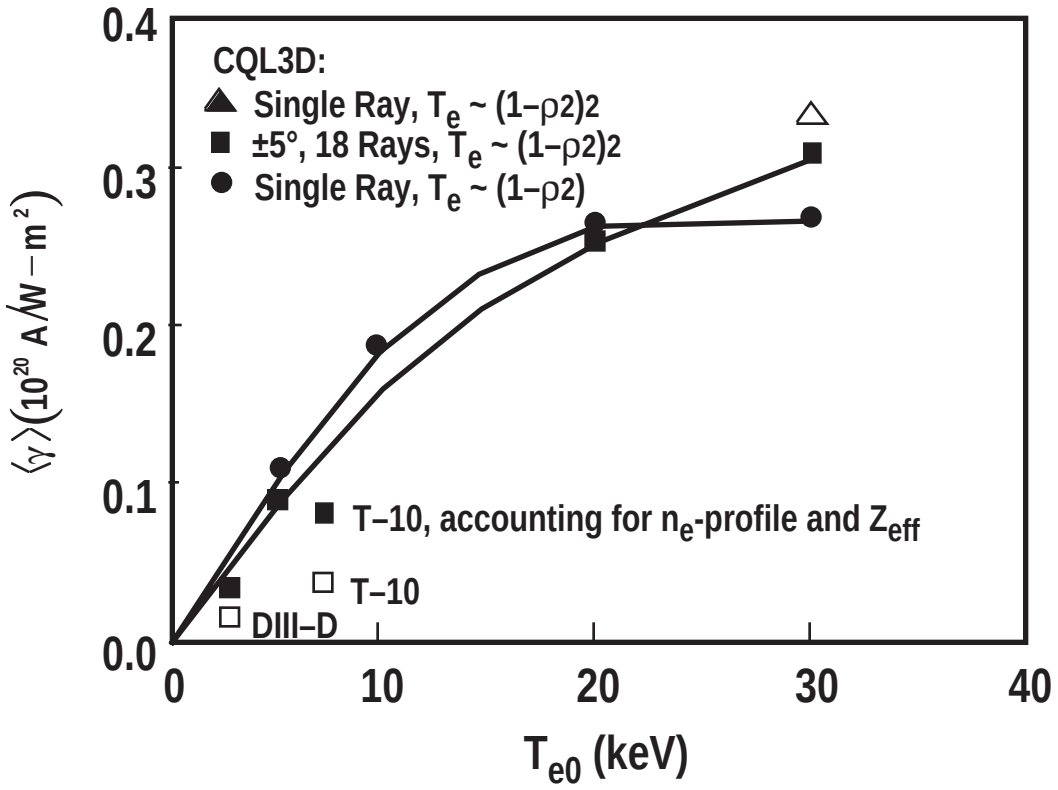

Fig. 15. Optimized CD efficiency $\langle\gamma\rangle_{opt}$ versus central plasma temperature for the 24 MA target plasmas. Curves are shown for single ray models for two different temperature profiles, and for a model with 10 deg divergence in the launch angle. Experimental results are shown for comparison.